Check for updates

Production of Janus/Hecate microfibers by microfluidic photopolymerization and evaluation of their potential in dye removal†

Wasif Razzaq,[ab] Christophe Serra*[a] and Delphine Chan-Seng [ID] *[a]

The microfluidic production of Janus/Hecate polymer microfibers with well-defined interfaces from miscible phases is reported. The process offers tunability of the width and composition of each part of the fibers by controlling the flow rate and nature of the monomers in a single step. The enhanced performances of the fibers are outlined for the simultaneous removal of dyes of opposite charges using amphoteric Janus fibers.

Microfibers have gained significant attention due to their potential in applications such as biomedicine[1] and sensors,[2,3] mainly because of their high surface to volume ratio. The development of structurally anisotropic microfibers increasingly strives to achieve fibers of different chemical natures and physical properties to overcome the limited performances of fibers based on a single material.[4,5] Among them, Janus fibers represent a great opportunity to access new properties and applications, but the routes to prepare them are still limited. Most reports focus on electrohydrodynamic processes including side-by-side electrospinning,[6–11] conjugate electrospinning,[12] microfluidic electrospinning,[13] and other conventional techniques such as direct jetting[14] and melt spinning.[15] Their main limitations are (i) access to diameters in the submicrometer range only, (ii) the incompatibility with biological systems due to high voltage, temperature, and use of solvent, and (iii) the restriction to pre-existing polymers in the presence of a suitable solvent.

Microfluidic spinning is an emerging and promising technique for the continuous fabrication of microfibers. It proceeds by establishing co-flow between a core phase (Φ_{core}) that will form the fiber material and a sheath phase (Φ_{sheath}) that hydrodynamically "spins" the fiber thanks to a microfluidic device. This technique offers advantages over conventional ones such as complete control over the diameter/volume ratio by tuning the flow rates of both the core and sheath fluids,[16] multiple solidification methods,[3] easy hydrogel formation,[17] micro- to submicron size range,[18] and compatibility with biological systems.[19] Fibers produced by microfluidic spinning relying on immiscible fluids provide access to jetting conditions only in a very narrow range of flow rates to obtain fibers and thus the use of multiple core phases is limited due to the existence of very different interfacial tensions.[20–22] Reports using purely miscible core and sheath phases describe the preparation of only single and Janus fibers based on alginate[23–26] and also hollow[27] and mosaicked[24] fibers from poly(ethylene glycol) diacrylate to date. Janus fibers have a side-by-side arrangement joined at the interface with two parts of different compositions offering the possibility to develop materials with unique properties (*e.g.* differentiated encapsulation abilities and compartmentalized properties). However, their preparation from monomers using miscible fluids has not yet been reported even though this strategy would significantly widen the type of Janus fibers (chemical nature of the different phases, one-step production of hydrogel, *etc.*) that could be obtained.

Herein, we report the use of a side-by-side capillary-based microfluidic device operating with different miscible phases (core monomer phases) co-flowing with the continuous (sheath) phase to produce Janus and Hecate microfibers. Two photopolymerizable monomer systems were used as core phase 1 (Φ_{core1}) and core phase 2 (Φ_{core2}). Φ_{core1} was composed of tri(propylene glycol) diacrylate (TPGDA, 80%v), ethanol (20%v), and Irgacure 369 (3%w/v) as the photoinitiator, while Φ_{core2} was composed of NOA89 (photocurable acrylate-terminated prepolymer) (80%v) and ethanol (20%v). Poly(ethylene glycol) with a molecular weight of 300 g mol^{-1} (PEG300) was used as the sheath phase. The core phases were injected at specific flow rates through capillary 1 and capillary 2 arranged side-by-side using syringe pumps (Fig. 1a). Φ_{core1} and Φ_{core2} exited at the tip of their respective capillary and got in contact with each other
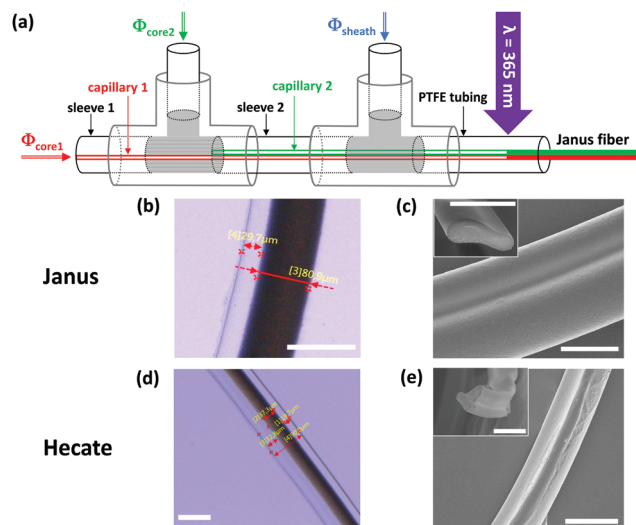
[a] *Université de Strasbourg, CNRS, Institut Charles Sadron UPR22, F-67000 Strasbourg, France. E-mail: ca.serra@unitra.fr delphine.chan-seng@ics-cnrs.unistra.fr*

[b] *Department of Materials, National Textile University, Sheikhupura Road, Faisalabad, 37610, Pakistan*

† Electronic supplementary information (ESI) available. See DOI: 10.1039/d2cc00214k
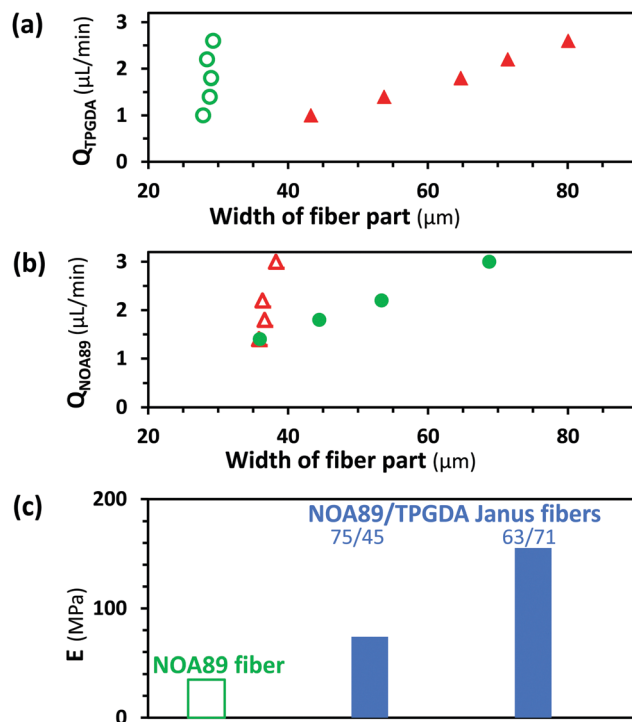
Fig. 1 Janus and Hecate fibers prepared using PEG300 as the sheath phase: (a) schematics of the microfluidic side-by-side capillaries system used to produce Janus fibers using TPGDA and NOA89 as core phases and the characterization of Janus (b and c) and Hecate (d and e) fibers by numerical (b and d, poly(TPGDA) observed in dark color) and scanning electron (c and e, fiber cross-section in inset) microscopies. Scale bars = 100 µm.

Fig. 2 Janus fibers from NOA89/TPGDA: (a) effect of Q_{TPGDA} on the width of the poly(TPGDA) part (▲) and cured NOA89 part (○) of Janus fibers for Q_{NOA89} = 1.0 µL min^{-1}, (b) effect of Q_{NOA89} on the width of the poly(TPGDA) part (△) and cured NOA89 part (●) for Q_{TPGDA} = 0.5 µL min^{-1}, and (c) comparison of the elastic modulus (E) of pure crosslinked NOA89 fibers with crosslinked NOA89/poly(TPGDA) Janus fibers by DMA.

spontaneously forming two parallel streams of monomers due to the shear imposed by the sheath fluid flow and their laminar flows (ESI,† Fig. S1). A second T-junction afforded the introduction of Φ_{sheath} using another syringe pump. Exiting this T-junction into PTFE tubing, the monomer streams were photo-polymerized using a UV lamp operating at a wavelength of 365 nm. The polymerized microfibers were collected into a water bath and washed with water and ethanol to remove the residual PEG (Φ_{sheath}) present at the surface of the fibers before air-drying them overnight. The fibers were produced using a flow rate of Φ_{core1}, Φ_{core2}, and Φ_{sheath} (Q_{TPGDA}, Q_{NOA89}, and Q_{sheath}) of 2.6, 1.0, and 700 µL min^{-1}, respectively. The fibers were characterized using numerical and scanning electronic microscopies (Fig. 1b and c) exhibiting the two distinct parts composing the Janus fibers and no significant degradation of the fibers after 8 months (ESI,† Fig. S2). Furthermore, an arrangement of three side-by-side capillaries was obtained by adding another T-junction and sleeve arrangement to the capillary-based microfluidic system shown in Fig. 1a. Hecate microfibers composed of three different materials originating from three monomers, i.e. TPGDA, NOA89, and poly(ethylene glycol) diacrylate with a molecular weight of 575 g mol^{-1} (PEGDA575), delivered through syringe pumps were prepared in a similar manner with a flow rate equal for all three core phases of 0.7 µL min^{-1} and Q_{sheath} = 1200 µL min^{-1}. Numerical and scanning electronic microscopies (Fig. 1d and e) showed the three phases of the Hecate fiber that were well-merged.

The morphological characteristics of Janus fibers (e.g. diameter) can be tuned by varying the volume contribution of each individual core phase as reported for electrospinning.[6] The flow rate of one of the core phases, either Q_{TPGDA} or Q_{NOA89}, was

varied while keeping constant the flow rate of the other core phase. For each experiment, the widths of both parts of the Janus fiber were measured by numerical microscopy (ESI,† Fig. S3) and their variations are plotted (Fig. 2a and b). The width and therefore the volume of each part of the fiber increased with an increase in the flow rate of the respective monomer as we reported for single fibers.[26] Due to the faster diffusion of the less viscous core phase into Φ_{sheath}, the corresponding part of the Janus fiber had a larger diameter (i.e. TPGDA). However, as expected, the part of the Janus microfiber with a constant monomer flow rate showed almost the same width. This clearly demonstrated that the individual flow rate of the core phases can control the volume of each part of the Janus fiber. Dynamic mechanical analysis (DMA) was performed on NOA89/TPGDA Janus microfibers to determine their elastic modulus and compare them to fibers that are solely composed of NOA89 having a diameter of 162 µm (Fig. 2c). Two Janus microfibers obtained from different ratios of core phase flow (i.e. 3.5/1.5 and 3/2.5) affording fibers with different widths (75/45 µm and 63/71 µm) were considered. The presence of TPGDA increased noticeably the elastic modulus of the pure NOA fiber (35 MPa) by almost twice for NOA89/TPGDA 75/45 (74 MPa) and up to five-fold for NOA89/TPGDA 63/71 (155 MPa). The results could not be compared to pure TPGDA fibers due to their high fragility rendering the DMA measurement not possible. The mechanical properties of a microfiber could be thus easily

tuned according to the needs of the application by producing Janus fibers from two materials having different mechanical properties. It is worth noticing that all the images presented in this work for the Janus microfibers as well as mechanical tests revealed no delamination of the microfibers. This probably originated from the interdiffusion of the monomer phases in each other during the co-flow of the core phases, which upon UV-induced polymerization strongly linked the materials together. This is another advantage of the microfluidic spinning technique, which allows starting from miscible monomer phases.

To evaluate the robustness of the microfluidic spinning technique, a library of Janus microfibers (Fig. S4, ESI†) was produced using different acrylic monomers including NOA74 (another photocurable acrylate prepolymer), acrylamide (Am), N-isopropyl acrylamide (NIPAm), poly(ethylene glycol) diacrylate with a molecular weight of 400 g mol^{-1} (PEGA400), n-butyl acrylate (n-BA), and $tert$-butyl acrylate ($tert$-BA). In the case of monovinylic monomers, 4 mol% of crosslinker was added (methyl bisacrylamide (MBA) for Am, PEGDA250 for n-BA and $tert$-BA) to ensure that the fibers were stable. All the combinations considered showed a clear interface between the two parts of the Janus fibers without delamination regardless of their different chemical natures (hydrophilic, hydrophobic, $etc.$). Amphoteric Janus fibers were thus prepared using an anionic monomer (acrylic acid, AA, 80 v% in water) as Φ_{core1} and a cationic one ((2-dimethylamino) ethyl acrylate, DMAEA, 80 v% in water) as Φ_{core2} (Q_{core1} = 1.5 μL min^{-1}, Q_{core2} = 3.0 μL min^{-1}, Q_{sheath} = 550 μL min^{-1}). Irgacure 2959 (4 wt/v%) was used as a photoinitiator and MBA as crosslinker. These fibers were investigated for their potential to simultaneously remove cationic and anionic dyes from a solution of different dyes. The dye removal efficiency (RE%) and the associated kinetics were conducted by immersing the fibers into a solution of 20 mg L^{-1} of either methylene blue (MB, cationic dye) or alizarin red S (AR, anionic dye) at 20 °C. An aliquot of the solution was withdrawn from the fiber solution at predetermined times for analysis using visible spectroscopy (664 nm for MB and 406 nm for AR). RE% was calculated for each dye and each time point (ESI,† Fig. S5) permitting it to be determined that the equilibrium was reached after 150 and 300 min for AR and MB, respectively, reaching a maximal RE% of 80 and 99%, respectively. The adsorption mechanism was further studied by considering the pseudo-first-order and pseudo-second-order adsorption models (ESI,† Fig. S6) exhibiting a better fit for the latter one with theoretical and experimental values of the adsorption capacity at equilibrium (q_e) relatively close for both dyes (ESI,† Table S1). These results indicated that the adsorption of MB and AR could be attributed to the electrostatic attractions of oppositely charged active sites on the fibers.[28] The adsorption capacity (q_e) for both dyes increased with an increase in the initial concentration of the dye (Fig. 3a): at lower concentrations, the increase was steeper approaching a plateau value at higher concentrations. Higher adsorption capacity at high concentrations is due to the presence of a large concentration gradient of dye molecules and adsorbents sites, which
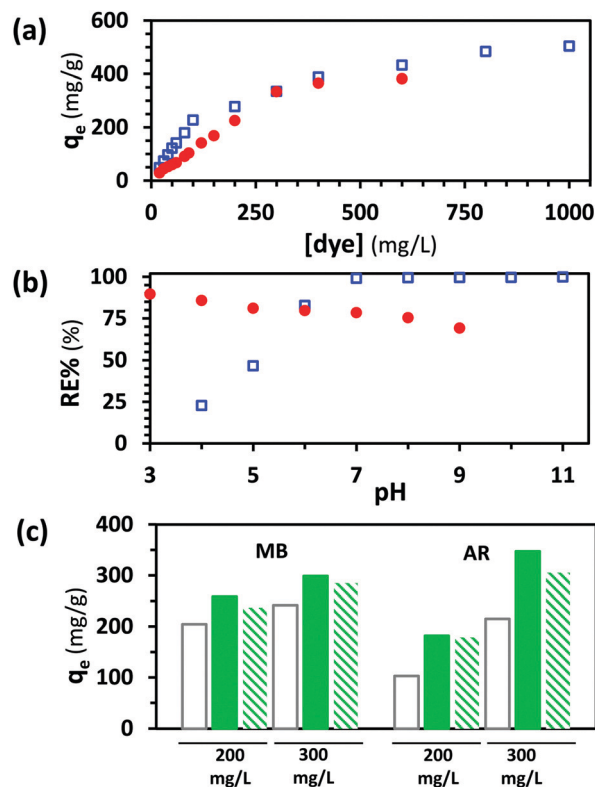

Fig. 3 Amphoteric AA/DMAEA Janus fibers and their capacity to adsorb dyes (MB = methylene blue = □, AR = alizarin red S = ●): effect of the (a) initial dye concentration on the adsorption capacity (q_e) and (b) pH on the dye removal efficiency (RE%), and (c) comparison of the fibers with a single part of a copolymer of AA and DMAEA (empty bars, grey border) with Janus fibers (green bars) when exposed to a single dye (filled) and both dyes (diagonal stripes) at 200 and 300 mg L^{-1} of dye.

results in an increase in the mass transfer between the adsorbent and dye molecules due to larger electrostatic attractions.[29] To evaluate the maximum adsorption capacity of the amphoteric Janus fibers, surface properties and interaction of the dye molecules with Janus fibers, the Langmuir and Freundlich isotherm models were applied to the data represented in Fig. 3a (ESI,† Fig. S7 and Table S1). The data better fitted to the Langmuir isotherm for both dyes showing that the adsorption followed a monolayer homogenous mechanism, and the separation constant (R_L) was between 0 and 1 for both dyes (ESI,† Table S2) showing the higher affinity and favorability of adsorption of dyes with the adsorbent.[30] Furthermore, the favorability of adsorption of MB and AR was confirmed through the Freundlich isotherm model, where the value of n for both the dyes was found to be in the region $0 < n < 10$. Another parameter of interest is the pH of the solution that was varied between 3 and 11 (Fig. 3b and ESI,† Fig. S8). The adsorption of MB increased from pH 4 to 7 reaching 100% of RE% and maintaining a plateau for higher values of pH. The decrease in adsorption at acidic pH was attributed to the protonation of the carboxylic acid groups reducing the charges accessible for adsorption of the dye at the surface of the poly(AA) part of the Janus fibers. Conversely, the adsorption of AR decreased

with increased pH values, which could be associated with the deprotonation of the amines and thus lowering the number of sites for AR to adsorb. The adsorption capacity of these fibers for either MB or AR is comparable or superior to materials reported in the literature (ESI,† Table S3) considering that most reports are on nanofibers which could have a strong influence on the adsorption capacity due to the higher surface to volume ratio. The adsorption capacity of these amphoteric Janus fibers was compared with fibers having a single part produced with both AA and DMAEA using the same feed composition of the monomers and flow rate conditions as for the Janus fibers (Fig. 3c). For each dye and concentration considered, the adsorption capacity of the amphoteric Janus fibers was observed to be superior. This could be due to the lower propensity of the comonomers to neutralize their charges in this structure due to the reduced area in which the monomers of opposite charges were in close proximity to the interface between the two parts of the Janus fibers. The simultaneous removal of both dyes by the amphoteric Janus fibers at pH 6.5 showed a slight decrease in adsorption capacity as compared to when only one dye was used (Fig. 3c) which could be due to (i) the specific pH requirement of each dye (pH = 7 for MB, pH = 6 for AR) and (ii) saturation and/or complexation of dyes in the solution leading to their precipitation (ESI,† Fig S9). Recycling capability is one of the crucial factors in evaluating the adsorbent performance. Cationic and anionic dyes could be desorbed using acidic and basic solutions. The fibers adsorbed with MB and AR were soaked in a 0.1 mol L^{-1} solution of hydrochloric acid and potassium hydroxide. Four cycles of adsorption–desorption were performed showing a very slight decrease in adsorption efficiency without affecting the appearance of the fibers (ESI,† Fig. S10). The decrease may be due to incomplete desorption of adsorbate and loss of active sites during regeneration associated with the protonation and deprotonation of the carboxylic acid and amine groups.[28]

In summary, Janus and Hecate microfibers were successfully produced using a simple microfluidic spinning technique. Miscible core and sheath phases were considered to avoid the formation of droplets associated with the interfacial forces among immiscible phases. The width, and thus the volume, of each individual part of the Janus microfibers can be easily tuned by altering the flow rate of one of the monomer phases. Janus microfibers of various chemical natures were successfully prepared to offer systems with increased mechanical properties and adjustable properties. Furthermore, the use of Janus fibers conversely to fibers constituted of a single part with the comonomer composition showed superior performances as illustrated for dye removal. These results pave the way to the development of multiphase microfibers for a wide range of applications, illustrated here with amphoteric Janus fibers that could be used for the simultaneous removal of positively and negatively charged species for water depollution.

Conflicts of interest

There are no conflicts to declare.

Notes and references

1 J. Cheng, Y. Jun, J. Qin and S. H. Lee, *Biomaterials*, 2017, **114**, 121–143.
2 J. Lou, Y. Wang and L. Tong, *Sensors*, 2014, **14**, 5823–5844.
3 X. Y. Du, Q. Li, G. Wu and S. Chen, *Adv. Mater.*, 2019, **31**, e1903733.
4 M. Akella, S. Shabaniverki and J. J. Juárez, *RSC Adv.*, 2020, **10**, 434–443.
5 Q. Huang, F. He, J. Yu, J. Zhang, X. Du, Q. Li, G. Wang, Z. Yu and S. Chen, *J. Mater. Chem. B*, 2021, **9**, 2727–2735.
6 G. Chen, Y. Xu, D. G. Yu, D. F. Zhang, N. P. Chatterton and K. N. White, *Chem. Commun.*, 2015, **51**, 4623–4626.
7 D. G. Yu, C. Yang, M. Jin, G. R. Williams, H. Zou, X. Wang and S. W. Bligh, *Colloids Surf., B*, 2016, **138**, 110–116.
8 J. Knapczyk-Korczak, J. Zhu, D. P. Ura, P. K. Szewczyk, A. Gruszczyński, L. Benker, S. Agarwal and U. Stachewicz, *ACS Sustainable Chem. Eng.*, 2020, **9**, 180–188.
9 M. Wang, D. Li, J. Li, S. Li, Z. Chen, D.-G. Yu, Z. Liu and J. Z. Guo, *Mater. Des.*, 2020, **196**, 109075.
10 J. Yang, K. Wang, D. G. Yu, Y. Yang, S. W. A. Bligh and G. R. Williams, *Mater. Sci. Eng., C*, 2020, **111**, 110805.
11 X. Cao, J. Deng and K. Pan, *Adv. Fiber Mater.*, 2020, **2**, 85–92.
12 J. Tian, Q. Ma, W. Yu, D. Li, X. Dong, G. Liu and J. Wang, *Mater. Des.*, 2019, **170**, 107701.
13 Y. Srivastava, M. Marquez and T. Thorsen, *Biomicrofluidics*, 2009, **3**, 12801.
14 Z.-C. Yao, J.-C. Wang, B. Wang, Z. Ahmad, J.-S. Li and M.-W. Chang, *J. Drug Delivery Sci. Technol.*, 2019, **50**, 372–379.
15 L. Ionov, G. Stoychev, D. Jehnichen and J. U. Sommer, *ACS Appl. Mater. Interfaces*, 2017, **9**, 4873–4881.
16 A. L. Thangawng, J. P. B. Howell, C. M. Spillmann, J. Naciri and F. S. Ligler, *Lab Chip*, 2011, **11**, 1157–1160.
17 R. Utoh, S. Enomoto, M. Yamada, K. Yamanaka, Y. Yajima, K. Furusawa and M. Seki, *Mater. Sci. Eng., C*, 2021, **129**, 112417.
18 S.-K. Chae, E. Kang, A. Khademhosseini and S.-H. Lee, *Adv. Mater.*, 2013, **25**, 3071–3078.
19 Y. Cheng, Y. Yu, F. Fu, J. Wang, L. Shang, Z. Gu and Y. Zhao, *ACS Appl. Mater. Interfaces*, 2016, **8**, 1080–1086.
20 J. K. Nunes, H. Constantin and H. A. Stone, *Soft Matter*, 2013, **9**, 4227–4235.
21 W. Lan, Y. Du, X. Guo, A. Liu, S. Jing and S. Li, *Ind. Eng. Chem. Res.*, 2017, **57**, 212–219.
22 A. Perazzo, J. K. Nunes, S. Guido and H. A. Stone, *Proc. Natl. Acad. Sci. U. S. A.*, 2017, **114**, E8557–E8564.
23 W. Jeong, J. Kim, S. Kim, S. Lee, G. Mensing and D. J. Beebe, *Lab Chip*, 2004, **4**, 576–580.
24 S. Cho, T. S. Shim and S.-M. Yang, *Lab Chip*, 2012, **12**, 3676–3679.
25 M. A. Daniele, K. Radom, F. S. Ligler and A. A. Adams, *RSC Adv.*, 2014, **4**, 23440–23446.
26 W. Razzaq, C. A. Serra, L. Jacomine and D. Chan-Seng, *J. Taiwan Inst. Chem. Eng.*, 2022, **132**, 104215.
27 C.-H. Choi, H. Yi, S. Hwang, D. A. Weitz and C.-S. Lee, *Lab Chip*, 2011, **11**, 1477–1483.
28 A. Shen, X. Liao and Y. Li, *Colloids Surf., A*, 2021, **623**, 126666.
29 R. B. Gapusan and M. D. L. Balela, *Mater. Chem. Phys.*, 2020, **243**, 122682.
30 C. Lei, F. Wen, J. Chen, W. Chen, Y. Huang and B. Wang, *Polymer*, 2021, **213**, 123316.